Atomic Force Microscopy−Scanning Electrochemical Microscopy: Influence of Tip Geometry and Insulation Defects on Diffusion Controlled Currents at Conical Electrodes

ARTICLE *in* ANALYTICAL CHEMISTRY · MARCH 2011

Impact Factor: 5.64 · DOI: 10.1021/ac103083y · Source: PubMed

8 AUTHORS, INCLUDING:

Amra Avdic
TU Wien
7 PUBLICATIONS **46** CITATIONS
SEE PROFILE

Alois Lugstein
TU Wien
129 PUBLICATIONS **1,726** CITATIONS
SEE PROFILE

Ilya Pobelov
Universität Bern
40 PUBLICATIONS **972** CITATIONS
SEE PROFILE

analytical chemistry

ARTICLE

pubs.acs.org/ac

Atomic Force Microscopy-Scanning Electrochemical Microscopy: Influence of Tip Geometry and Insulation Defects on Diffusion Controlled Currents at Conical Electrodes

Kelly Leonhardt,[†] Amra Avdic,[‡] Alois Lugstein,[‡] Ilya Pobelov,[§] Thomas Wandlowski,[§] Ming Wu,[⊥] Bernhard Gollas,[⊥,¶] and Guy Denuault*[,†]

[†]School of Chemistry, Highfield Campus, University of Southampton, Southampton, SO17 1BJ, United Kingdom

[‡]Solid State Electronics Institute, Vienna University of Technology, Floragasse 7, 1040 Vienna, Austria

[§]Department of Chemistry and Biochemistry, University of Bern, Freiestrasse 3, CH-3012 Bern, Switzerland

[⊥]CEST Competence Centre for Electrochemical Surface Technology, Viktor-Kaplan-Strasse 2, Wiener Neustadt, Austria

[¶]Institute for Chemistry and Technology of Materials, Graz University of Technology, Stremayrgasse 9, 8010 Graz, Austria

Supporting Information

ABSTRACT: Numerical simulations were performed to predict the amperometric response of conical electrodes used as atomic force microscopy-scanning electrochemical microscopy (AFM-SECM) probes. A simple general expression was derived which predicts their steady state limiting current as a function of their insulation sheath thickness and cone aspect ratio. Simulated currents were successfully compared with experimental currents. Geometrical parameters such as insulation angle and tip bluntness were then studied to determine their effect on the limiting current. Typical tip defects were also modeled using 3D simulations, and their influence on the current was quantified. Although obtained for SECM-AFM probes, these results are directly applicable to conical micro- and nanoelectrodes.

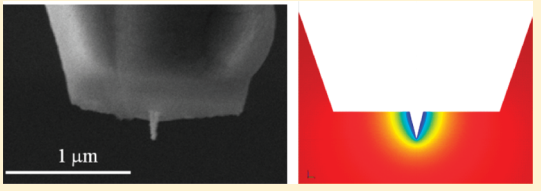

The need to study and image surfaces with a submicrometer resolution led to the combination of scanning electrochemical microscopy (SECM) and atomic force microscopy (AFM). In SECM, a microelectrode is scanned over a surface to map its reactivity,[1] whereas in AFM, a sharp tip at the end of a cantilever is used to determine the topography of a surface on the atomic scale.[2] The hybrid AFM-SECM technique was first introduced in 1996 when an entirely electroactive AFM cantilever was used to electrochemically induce the dissolution of a crystal and to record its topography.[3] A similar probe was later used in the study of conducting and insulating substrates.[4] The idea of combining an AFM probe with a microelectrode near its tip apex was then introduced by Kranz et al. as a sharp insulating cone protruding from a square electroactive frame; it was fabricated by coating a whole AFM cantilever-tip assembly first with an electroactive layer and then with an insulation layer and finally milling around the apex with a focused ion beam (FIB) to form the tip.[5−7] The same fabrication method was also used to make integrated ring electrodes.[8] Other geometries have since been investigated. Macpherson et al. fabricated probes by insulating flattened etched Pt microwires, leaving the end exposed to act as an electrode.[9,10] Microdisc electrodes have also been used: a tip made of a Pt microwire surrounded by an insulation sheath with a separate AFM tip in the insulation was developed to study localized corrosion.[11−13]

With such tips being difficult and expensive to make, numerical simulations have become an important part of AFM-SECM studies. Sklyar et al.[14] modeled diffusion toward frame shaped electrodes in 3D using the boundary element method. Simulations of entirely insulating cantilevers of different shapes have been performed to determine their effect when approaching conducting islands.[15] Diffusion toward entirely conducting cantilevers has been modeled in transient 3D simulations, when the probes were held above insulating surfaces and above conducting islands within insulating surfaces.[4] Some simulations even took into account the flow when scanning the surfaces.[12,16] Conical electrodes with conical insulation as seen in SECM/AFM have been previously simulated in 2D and 3D, and a simple defect was studied to determine its effect on the limiting current.[17,18]

Dickinson et al.[19] studied the amperometric response of conical tips using both potential step and potential sweep experiments and determined trends in the response as a function of the cone half angle; the maximum current density was found to be for a half angle of 75°. Sklyar et al.[20] simulated conical electrodes taking into account the tip bluntness and different aspect ratios for a fixed insulation sheath size and angle. Approach curves were generated to determine the effect of the aspect ratio on the current when approaching a substrate. The sharper cones, with higher aspect ratios, were shown to be less effective for SECM measurements, as no contrast was observed

Received: November 23, 2010
Accepted: March 7, 2011
Published: March 28, 2011

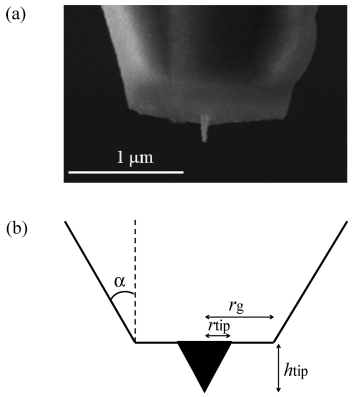

Figure 1. (a) Micrograph of a conical electrode with conical insulation, as used in AFM-SECM probes. (b) The "perfect" conical tip defined by the height and radius of the electroactive cone, h_{tip} and r_{tip}, and the radius of the insulation, r_g. The insulation sheath has the same half angle α with the vertical as the electroactive cone.

in SECM feedback measurements. With decreasing aspect ratios, the behavior of the protruding tips was reported to get closer to that of microdisc electrodes. Zoski et al.[21] derived from simulations a fitting expression for the steady state limiting current of conical electrodes with cylindrical insulation when varying the insulation thickness for a range of aspect ratios. These parameters were also varied when generating approach curves.[22]

Conical electrodes with conical insulation have been used before in SECM[23] and AFM-SECM.[17,18] However, in these cases, the steady state current measured at the electrode was compared to the current using the expression derived by Zoski and Mirkin,[21] which was for a conical electrode with cylindrical insulation. Gullo et al.[17] attempted to remedy this by simulating a conical electrode with conical insulation and a conical electrode with cylindrical insulation. The two results were compared, and the relative difference between the two was quantified. This was then used to adjust Zoski and Mirkin's expression for all tips.

The main objective of this paper is to provide anyone using conical AFM-SECM tips or conical microelectrodes with a simple and general expression to calculate the diffusion controlled limiting current at a conical electrode for any cone angle and any insulating sheath thickness. The second objective of this Article is to provide a quantitative assessment of the influence of geometric parameters (bluntness or insulation angle) and of defects (gap in the insulation, uneven insulation or off centered tip) on the limiting current. These results will guide the design of optimum tip geometries and help decide whether defective tips should be discarded or used.

EXPERIMENTAL AND SIMULATION DETAILS

In our work, a commercially available AFM cantilever is first covered with a layer of electroactive material such as gold or a commercially available BDD-coated AFM cantilever is used. The cantilevers are then coated with a layer of insulation such as SiN. Finally, a sacrificial Cr layer is deposited on the probe. The insulation and sacrificial layers are partially removed from the tip apex using focused ion beam (FIB) to expose the insulation, which is subsequently etched by reactive ion etching (RIE), thus revealing the electroactive area. After the tip exposure, the Cr layer is removed. The fabrication process, further detailed by Avdic et al.,[24] produces conical tips with conical insulation sheath, as shown in Figure 1a.

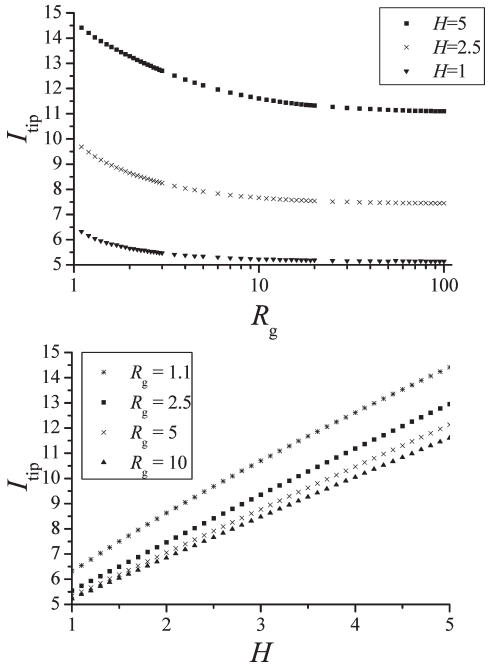

Figure 2. (a) Plot of the dimensionless tip current against the insulation sheath thickness R_g for different values of H. (b) Plot of the dimensionless tip current as a function of the aspect ratio H for different values of R_g.

The electrodes were characterized by cyclic voltammetry in 1 mM solution of ferrocenemethanol (FcMeOH) in either 0.1 M KNO_3 or 0.1 M H_2SO_4 using an Autolab PGSTAT 128N potentiostat (Utrecht, Netherlands) and a custom built bipotentiostat (G. Meszaros, T. Pajkossy, Budapest, Hungary). The counter electrode was a Pt wire, and the quasi reference electrode was either an Ag or a Pt wire, the potential of which was calibrated with respect to a reference electrode such as Ag/AgCl.

Three numerical methods have mostly been used to solve electrochemistry problems: finite differences,[25,26] finite elements, and boundary element[14,27−29] methods. The finite element method was chosen for the present study because it offers an extremely versatile mesh particularly suited to electrochemistry models which tend to have complex geometries and difficult boundary conditions. This method has, therefore, often been used in electrochemistry.[4,12,15,17,21,30,31] The simulations were run from MATLAB, using COMSOL Multiphysics v.3.5a as the finite element solver, on a Windows 64 bit, Intel Xeon CPU with 2.66 GHz and 11.9 GB of RAM. Details of the modeling conditions and mesh used can be found in the Supporting Information, as well as the validation of the approach by comparison with microelectrode geometries previously simulated or with known analytical solutions.

RESULTS AND DISCUSSION

Perfect Conical Tip. To derive a general expression for the steady state current at a conical electrode in the bulk solution, the response of a "perfect tip", a symmetrical tip with no radius of curvature, see Figure 1b, was modeled. Its geometry was defined by three parameters, namely, r_{tip}, the radius of the electroactive cone, h_{tip}, the height of the electroactive cone, and r_g, the radius of the insulation sheath, and by the assumption that the latter forms the same half angle α with the vertical as the conical

electrode. The models built were dimensionless, with distances divided by the radius r_{tip} of the electroactive cone and concentrations by the bulk concentration. The simple geometry, now characterized by $H = h_{tip}/r_{tip}$, the aspect ratio of the conical electrode, and $R_g = r_g/r_{tip}$, the radius of the insulation sheath, allows a 2D axi-symmetric model, thus significantly saving on computational effort. The steady state limiting current at the electrode in the bulk was defined as $I_{tip} = i_{tip}/nFDc^b r_{tip}$, with the limiting current at the electrode i_{tip}, the number of electrons n, Faradays constant F, the diffusion coefficient D, the bulk concentration c^b, and the radius of the electroactive cone r_{tip}, as detailed in SI 2, Supporting Information.

The simulations were run for aspect ratios $H = 1$ to $H = 5$, with increments of 0.1, and for each aspect ratio, the dimensionless radius of the insulation sheath, R_g, was varied from 1.1 to 100. The dependence of the dimensionless current I_{tip} on R_g for different H can be seen in Figure 2a. Whatever the aspect ratio, the curves follow the same trend, with smaller values of R_g providing significant back diffusion around the insulation sheath and producing a larger current. As the insulation sheath becomes thicker, the diffusion layer spreads radially leading to a decrease in current. Eventually, the current reaches a plateau when the insulation is so thick that any increase in thickness does not affect the diffusion to the electrode. Note that this is reached at lower values of R_g for tips with smaller aspect ratios as the exposed area is smaller. The dependence of the current on the aspect ratio H for different values of R_g is shown in Figure 2b. Over the range considered, there is an almost linear relationship between the current and the aspect ratio. However, the dependence on H decreases with thicker insulation due to the increased blocking of diffusion by the insulator, as seen by the loss of steepness of the curves with increasing R_g. As a result, high aspect ratio tips are much more sensitive to the insulation thickness.

An expression of the form $I_{tip} = A + B \times (R_g + C)^{-D}$ was then fitted for each value of H. After analysis, it was found that the coefficients A, B, C, and D were simple first and second degree polynomial functions of H and that the steady state current for any conical electrode described by its aspect ratio H and insulation sheath thickness R_g could therefore be calculated from the following expression:

$$i_{tip} = nFDc^b r_{tip}\left[A_H + B_H(R_g + C_H)^{-D_H}\right] \quad (1)$$

where n is the number of electrons in the reaction, F is Faraday's constant, D is the diffusion coefficient, c^b is the bulk concentration, and r_{tip} is the radius at the base of the electroactive cone. The four coefficients are given by

$$A_H = 1.47972H + 3.69141 \quad (2)$$

$$B_H = 0.12629H^2 + 0.65894H - 0.01259 \quad (3)$$

$$C_H = 0.0115H^2 + 0.25251H - 0.72687 \quad (4)$$

$$D_H = -0.00943H^2 + 0.08213H + 0.83038 \quad (5)$$

Equation 1 results from over 2000 simulations and fits the simulated current matrix within 0.38% on average. For H ranging from 1 to 5 and R_g from 1.1 to 100, the largest relative difference between eq 1 and the simulation is 0.93%, well within the range of typical experimental error at microelectrodes. Thus, eqs 1−5 provide a simple general expression which predicts the diffusion controlled current at a conical electrode for any aspect ratio and insulation sheath thickness. Other methods were investigated to derive a suitable fitting expression. However, none were as accurate as the fitting expression described above or as simple.

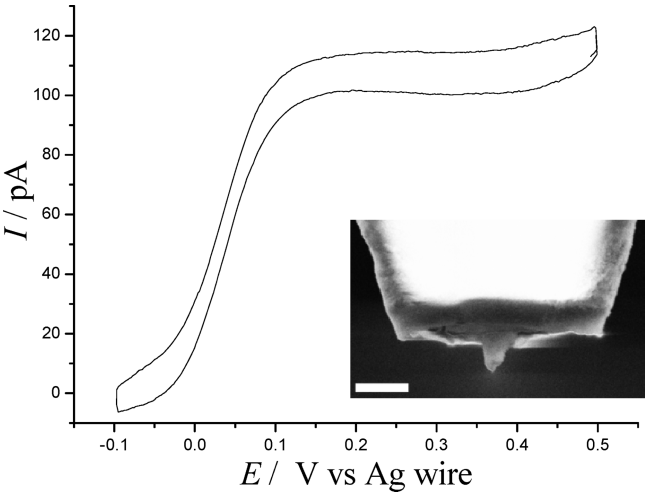

Figure 3. Voltammogram recorded with a gold cantilever in 1 mM FcMeOH + 0.1 M KNO_3 at 50 mV/s. The inset shows an SEM image of the Au tip where the scale bar represents 500 nm. Fabrication details are described in ref 24.

A typical conical tip fabricated in this study is shown in Figure 3. Its dimensions were found to be: radius of the electroactive cone r_{tip} = 240 nm, aspect ratio H = 1.8, and insulation sheath radius R_g = 4. With these parameters, eq 1 predicts a theoretical limiting current of 107 pA for a 1 mM solution of FcMeOH ($D = 6.7 \times 10^{-6}$ cm^2 s^{-1}), which is in very good agreement with the measured current, approximately 100 pA, from the experimental voltammogram shown in Figure 3.

The fabrication of these tips is, however, complex and defects inevitably occur. Considering the manufacturing costs involved, it is important to assess how defects affect the tip response and to determine whether a defective tip should be discarded or not. The next section considers typical defects encountered and quantifies their influence on the limiting current.

Influence of Tip Geometry and Insulation Defects

Effect of the Tip Bluntness. The tip cannot be perfectly conical, and a degree of bluntness at the apex, as depicted in Figure 4(a), must be considered. Commercial probes are sold with a guaranteed apex radius a, typically between 7 and 12 nm. As a result, conical tips with a base radius r_{tip} in the submicrometer range are expected to be affected by this parameter. The influence of the bluntness was simulated for a range of base radii. 2D axi-symmetric simulations were run using a tip apex radius a = 10 nm, which was deemed to be the standard value. The electroactive tip radius r_{tip} was varied from 10 nm, for which the tip is a cylinder, to 1 μm, the highest radius considered suitable for AFM-SECM. Three different aspect ratios were modeled: H = 1, H = 2.5, and H = 5. The relative difference between the current at the blunt tip and that at the perfect tip was evaluated for a wide range of tip aspect ratios and tip radii; a summary of the results is presented in Table 1.

The relative differences between a blunt tip and a perfect tip, Table 1, are always positive, as the blunt tip always produces a higher current. As expected, the larger the electrode, the smaller is the effect of the tip bluntness. Therefore, for electrode radii larger than 600 nm, the current will be enhanced by less than 1% compared to that at a perfect tip. As the electrode gets smaller, the

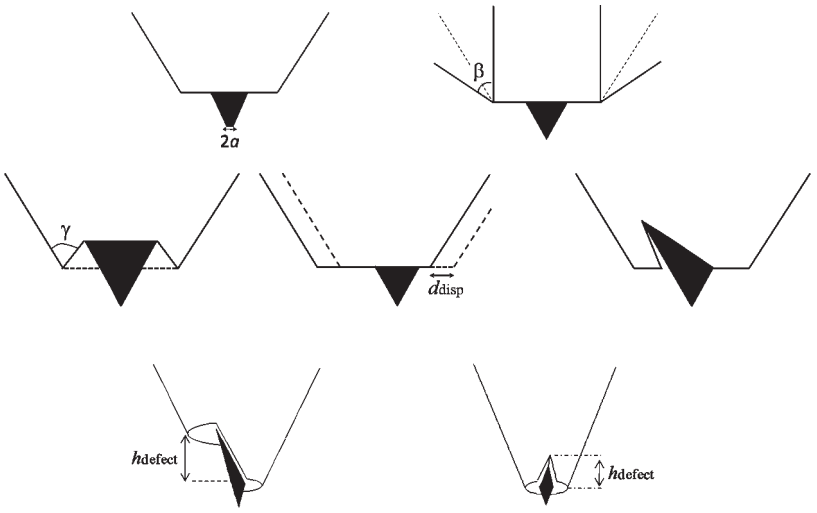

Figure 4. Schematic representations of common tip defects: (a) a blunt tip with apex radius a, (b) a tip with insulation angle β, (c) a tip with a defect in the insulation joining angle γ, where the dashed line represents the perfect insulation and the black area represents the electrode, (d) an off centered tip, where d_{disp} is the distance by which the insulation is displaced. The perfect insulation is represented by a dashed line. (e) A tip with a gap between the insulation and the electroactive area, (f) a tip with uneven insulation, with the electroactive area in black. h_{defect} is the height difference between the two levels of insulation. (g) A tip presenting a crack in the insulation. Here, h_{defect} is the height of the crack.

Table 1. Summary of the Relative Difference between the Current at a Blunt Tip (apex radius a = 10 nm) and That at a Perfect Tip (a = 0) for Different Aspect Ratios H and Electroactive Cone Radii r_{tip}

r_{tip} range	H = 1	H = 2.5	H = 5
600 nm ≤ r_{tip} < 1 μm	<1%	<1%	<1%
100 nm ≤ r_{tip} < 600 nm	<4%	<5%	<6%
60 nm ≤ r_{tip} < 100 nm	<8%	<9%	<9%
20 nm ≤ r_{tip} < 60 nm	<21%	<25%	<25%

relative difference becomes larger. For tips with radii smaller than 60 nm, the current is increased by at least 10%. The current calculated using the general expression, eqs 1−5, would, therefore, have to be corrected accordingly. Note that the greater the aspect ratio H, the more important is the effect of the bluntness on the limiting current. In summary, the bluntness of the tip must be taken into consideration when radii smaller than 100 nm are used, as the current will be increased by more than 5% compared to that of a perfect tip.

Effect of the Insulation Angle. The perfect insulation was considered to have the same angle with the vertical as the electroactive cone. However, in many cases, the insulation has a different angle to the electroactive cone. This geometry, shown in Figure 4b, was, therefore, further investigated by varying the insulation angle β from 0 to 90° (where 33.7° represents the perfect tip) for H = 1.5; the dependence of the limiting current at the electrode on the insulation angle β and the insulation sheath thickness R_g can be seen in Figure 5. When β = 0°, the insulation is cylindrical and the electrode has the geometry described by Zoski and Mirkin.[21] When β = 90°, the tip has an infinite insulation plane.

Not surprisingly, the relative difference between the current at the defective tip and the current at the perfect tip decreases when increasing the insulation sheath radius R_g. β has very little influence with large R_g due to the size of the insulation plane. However, for small values of R_g, the insulation angle controls the amount of back diffusion around the insulation sheath. For example, a tip of aspect ratio H = 1.5 and insulation angle β = 60° will have a

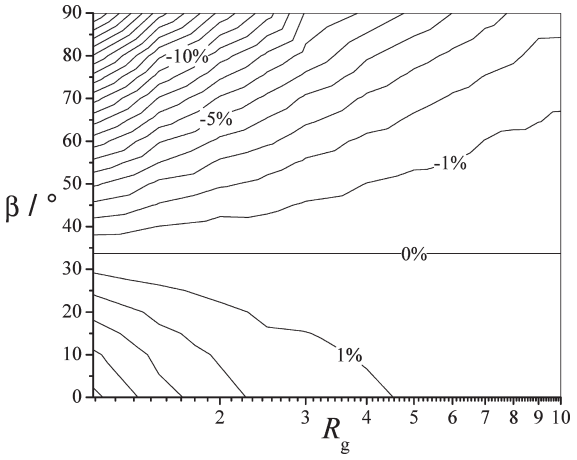

Figure 5. Contour plot of the relative difference (in %) between the dimensionless current at a tip with insulation angle β and the dimensionless current at a perfect tip (β = 33.7°), plotted as a function of the angle β and the insulation sheath thickness R_g. The contour interval is 1%.

current approximately 7.5% smaller than that at a perfect tip. Insulation angles larger than the perfect tip angle produce lower currents due to the diffusion layer being more spread. In contrast, smaller angles lead to increased currents as the diffusion is less hindered by the insulation. Although a large range of angles are considered, the angles most likely to be encountered (between 0° and 50° in SECM and 20° and 50° in SECM-AFM) result in a current increase or decrease of less than 6%.

Effect of the Insulation Joining Angle. A common defect of the insulation sheath observed is the insulation joining the electrode at an angle as depicted in Figure 4c. The perfect tip insulation forms a flat circular plane from which the conical electrode protrudes. However, defective insulation has been observed to form a crater around the electrode tip, as seen in Figure 4b in Gullo's paper,[17] or a "mound". This defect was simulated in 3D for a typical aspect ratio H = 1.5. The insulation

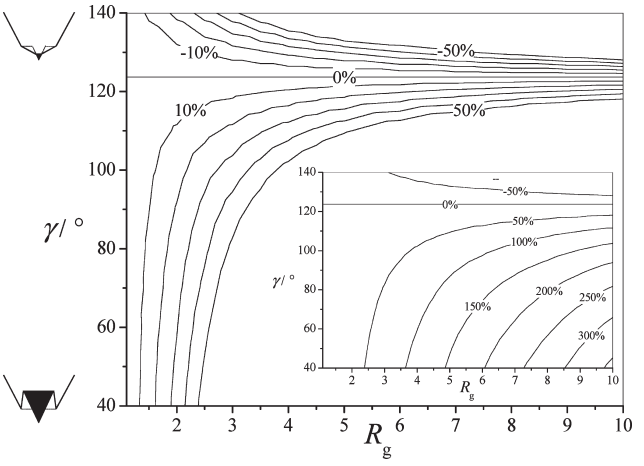

Figure 6. Plot of the relative difference (in %) between the dimensionless current at a tip with insulation joining angle γ and that at a perfect tip (γ = 123.7°). This is plotted as a function of the angle γ and the insulation sheath thickness R_g, with a contour interval of 10%. The inset shows the same plot on a different scale, with a contour interval of 50%. The two extreme cases are schematically represented on the left to illustrate the range of defects considered.

joining angle γ was varied from 40° to 140°; see extreme cases depicted in Figure 6, where 123.7° represents the perfect insulation. The insulation radius R_g was varied from 1.1 to 10. The limiting current was compared to the current of the perfect tip to determine the influence of this defect.

As expected, this defect has a large effect on diffusion toward the electrode, as shown in Figure 6. This is due to the large change in exposed area. For angles larger than the perfect tip angle, the insulation goes up near the tip, resulting in a smaller exposed area. Consequently, the current is much smaller. For angles smaller than the perfect tip angle, the current is much larger, as the electrode surface is now much bigger. The diffusion is, however, still partially blocked by the insulation crater. In practice, the current at the defective tip should be estimated as if working with a perfect tip (i.e., by picturing the insulation for a perfect tip and using this to calculate the electrode parameters), using eq 1 to determine the perfect tip current and then correcting for the angle of the crater using Figure 6. This study shows that even a small crater can result in a significant change in current; this would severely decrease the sensitivity of the tip for SECM measurements.

Effect of an off Centered Tip. A defect that can be encountered is the tip being off centered as shown in Figure 4d. Simulations were run in 3D for typical aspect ratios H = 1.5 and H = 2.5 and typical range of insulation sheath R_g= 1.1−10. The dimensionless displacement distance was varied from 0.1 to 8 in one direction, and the steady state limiting current was computed for each case. This was then compared to the perfect tip current. The largest relative difference for both aspect ratios was 4.2%, which is within experimental error. A worst case scenario was then modeled for R_g = 10, with the insulation displaced in both the x- and y-direction, leaving the electroactive tip at the extremity of the insulation plane. The current for this tip was 7.8% smaller than the current for the tip with perfect insulation. Therefore, even for the worse case, this defect does not have a large influence on the current at the electrode; this is partly due to the fact that, unlike other defects considered in this study, there is no increase in exposed electroactive area. The decrease in current

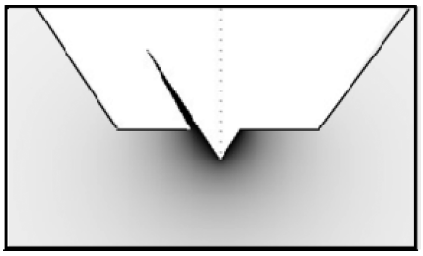

Figure 7. Vertical cross-section through the center of a tip with a gap in the insulation. The gray scale shows the concentration around the tip with black for the lowest and light gray for the largest concentrations.

due to the blocking of diffusion on one side is compensated by the increase in current caused by the back diffusion on the other side, resulting in a small change in current overall. This defect can, therefore, be ignored as it does not influence diffusion to the electrode much and is not expected to affect the resolution or sensitivity of the tip when imaging a surface.

Effect of a Gap between Insulation and Electrode. A common defect that can occur with the fabrication method used here is the presence of a small gap between the insulation and the electrode, increasing the exposed area, as depicted in Figure 4e. This has been previously studied in a 2D axi-symmetric configuration, where a small gap was modeled and shown to increase the current by only 3%.[17] Here, simulations were run for H = 1.5 and R_g = 5. The defect was characterized by the width of the gap at the insulation plane. The angle with the vertical formed by the fissure is 5° smaller than the half angle of the cone, resulting in a thin crack. The dimensionless defect width initially studied was 0.5, half the radius of the conical electrode. Three different cases were then studied: the gap in the insulation around the entire electrode, half the electrode, and a quarter of the electrode, as represented in Figure 4e. Compared to a perfect tip, a gap all around the cone increased the current by 10.2%, a gap around half the electrode increased the current by 5.6%, while a gap around only a quarter of the electrode increased the current by only 3%. Figure 7 displays a concentration profile for this example.

The main observation is that the concentration is at its minimum (black color) in the fissure. Only toward the opening of the gap does diffusion occur. This explains the small change in current observed: even though there is a large increase in exposed area, the insulation blocks diffusion from occurring inside the gap. Smaller sized gaps were then investigated for a gap surrounding the entire electrode: a dimensionless gap width of 0.2 was set, and the current was calculated to be 3.6% larger than the perfect tip current. Finally, the same problem was modeled for a defect width of 0.1, ten times smaller than the electrode radius. For this case, the current was 1.9% higher than that at the perfect tip current. This study shows that small gaps in the insulation do not have a large influence: the gaps are too small for diffusion to spread through the fissure, hence the relatively small effect on the current. For very large gaps, this example will get closer to the "crater" like insulation studied in the section Effect of the Insulation Joining Angle. However, for gaps smaller than half the radius of the electrode, the tip can still be used without the SECM resolution or sensitivity being compromised.

Effect of Uneven Insulation Coverage. Another defect that can occur during the fabrication method is uneven insulation around the cone; see Figure 4f. This defect, which was investigated for aspect ratio H = 1.5 and insulation sheath thickness R_g = 5, is

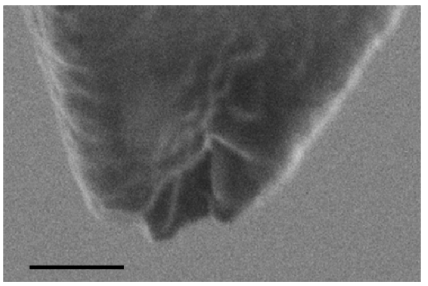

Figure 8. Micrograph of a tip with a crack in the insulation, with the scale bar representing 1 μm.

characterized by the height difference h_{defect} between the two "levels" of the insulation sheath. Due to the complexity of the geometry and the number of mesh elements, approximately 25×10^4, each individual simulation took between 1 and 2 h to solve. This was done for dimensionless height $H_{defect} = h_{defect}/r_{tip}$ ranging from 0.1 to 5. For a defect of height $H_{defect} = 2$, i.e., twice the radius of the electroactive cone, the limiting current produced was found to be 25% larger than that at the perfect tip. The maximum defect height modeled was $H_{defect} = 5$, for which the limiting current was calculated to be twice the limiting current of the perfect tip. This defect results in a large increase in exposed area, reflected in the measured current, which increases rapidly with larger H_{defect}. Both typical cases and an extreme case were modeled here. Typically, the defect height would be expected to be smaller than the diameter of the base of the cone; however, this still produces an increase of less than 25%. Any larger defect size would result in a significant loss in resolution, and the tip would not be usable.

Effect of a Crack in the Insulation Sheath. The final part of the investigation into defects concentrated on the insulation containing a crack as observed in Figure 8 and represented in Figure 4g. This defect is characterized by the dimensionless height of the defect H_{defect} and the width of the defect. Three different cases were simulated: $H_{defect} = 1$, 2, and 5 and the dimensionless current I_{tip} calculated for each.

In all three examples, the dimensionless width of the crack was fixed at 1. The first case led to a 12.5% increase in current, but the worst case produced a 40.5% increase in current. Unlike the example with the gap in the insulation, diffusion to the extra exposed area is not blocked; hence, the large increase in current is observed. This defect is, therefore, expected to greatly affect the resolution of the tip.

Effect of the Cantilever. The tips studied here are used in AFM-SECM and, therefore, are found at the end of cantilevers. For the completeness of the study, the presence of the cantilever had to be taken into consideration. Two types of cantilevers were investigated: the first is a cantilever with a cone height of 12 μm and an aspect ratio of $H = 1.5$, typical of those used in this project. The cantilever has a width of 50 μm and a thickness of 2 μm. A second cantilever consisting of a pyramidal tip of height 3.3 μm and cantilever thickness 0.7 μm was studied. The cantilever is expected to act as a shield above the tip and spread the diffusion, resulting in a smaller current at the electrode and a loss of resolution in SECM imaging. To quantify the effect of the cantilever, the smallest insulation thickness is considered ($R_g = 1.1$), as this will have the most back diffusion. A range of values of r_{tip} were modeled from 1 to 0.01 μm, and the largest relative difference in the current with and without cantilever was quantified. This was shown to be within 0.7% for cantilever 1 and 1.1% for cantilever 2 for tips with radii between 1 μm and 500 nm. Tips in AFM-SECM will have radii below 500 nm, for which the current was shown to decrease by less than 0.4%. With the largest perturbation producing a 1.1% decrease in current, the results show that the cantilever has a negligible effect with all the tips including those considered in AFM-SECM ($r_{tip} < 1$ μm). With a relative difference below 0.1%, the effect of the cantilever can be ignored when $r_{tip} < 200$ nm. While these results apply to a tip in the bulk, the influence of the cantilever is expected to be more important with decreasing tip to substrate distance.

CONCLUSION

The diffusion controlled current at conical microelectrodes employed as SECM-AFM tips was simulated. The simulation conditions were validated for several electrode geometries with known analytical solutions and with an adaptive finite element solver. A range of cone tip geometries and defects were considered, and their influence on the tip current was assessed by comparison with that at an ideal conical tip. This study has produced a simple expression capable of predicting the steady state current at a conical electrode with conical insulation, as a function of H, the aspect ratio of the cone, and R_g, the insulation sheath radius, valid for H ranging from 1 to 5 and R_g from 1.1 to 100. This expression fits within 1% of the simulated results. The tip bluntness was shown to be important when working with tip radii smaller than 100 nm; the insulation angle was found to be important for small values of R_g. Off centered tips were found to have little effect on the limiting current, with the worst case resulting in a decrease in current of less than 8%. The case of the insulation forming a crater around the electrode was shown to be the most important defect, with large changes in current due to the increase in exposed area and absence of blocking by the insulation layer. Finally, the presence of the cantilever was found to have negligible effect on the tip current in the bulk. The quantitative analysis of the tips performed here enables users to calculate the current at a defective tip using the expression derived from the perfect tip and readjusting it using the relative difference given.

These tips are used to image surfaces. It is, therefore, essential to study and understand their behavior close to the substrate. With this in mind, the current response of both perfect and defective tips will be modeled when holding or scanning the probe above a range of substrates at different tip−substrate distances. This work will be presented in a subsequent publication.

ASSOCIATED CONTENT

Supporting Information. Details of the numerical approach used, the description of the model conditions, and an example of a 3D mesh generated. This material is available free of charge via the Internet at http://pubs.acs.org.

AUTHOR INFORMATION

Corresponding Author

*E-mail: gd@soton.ac.uk. Phone: +44 2380 592154.

ACKNOWLEDGMENT

This work was funded by the COMET programme of the Austrian Research Advancement Agency (Österreichische Forschungsförderungsgesellschaft FFG), the government of

Lower Austria, the University of Bern, and the Swiss National Science Foundation

REFERENCES

(1) Bard, A. J.; Fan, F. R. F.; Kwak, J.; Lev, O. *Anal. Chem.* **1989**, *61* (2), 132–138.
(2) Binnig, G.; Quate, C. F.; Gerber, C. *Phys. Rev. Lett.* **1986**, *56* (9), 930–933.
(3) Macpherson, J. V.; Unwin, P. R.; Hillier, A. C.; Bard, A. J. *J. Am. Chem. Soc.* **1996**, *118* (27), 6445–6452.
(4) Holder, M. N.; Gardner, C. E.; Macpherson, J. V.; Unwin, P. R. *J. Electroanal. Chem.* **2005**, *585* (1), 8–18.
(5) Kranz, C.; Friedbacher, G.; Mizaikoff, B., *Anal. Chem.* **2001**, *73* (11), 2491-+.
(6) Lugstein, A.; Bertagnolli, E.; Kranz, C.; Kueng, A.; Mizaikoff, B. *Appl. Phys. Lett.* **2002**, *81* (2), 349–351.
(7) Kranz, C.; Kueng, A.; Lugstein, A.; Bertagnolli, E.; Mizaikoff, B. *Ultramicroscopy* **2004**, *100* (3−4), 127–134.
(8) Lugstein, A.; Bertagnolli, E.; Kranz, C.; Mizaikoff, B. *Surf. Interface Anal.* **2002**, *33* (2), 146–150.
(9) Macpherson, J. V.; Unwin, P. R. *Anal. Chem.* **2000**, *72* (2), 276–285.
(10) Macpherson, J. V.; Unwin, P. R. *Anal. Chem.* **2001**, *73* (3), 550–557.
(11) Davoodi, A.; Pan, J.; Leygraf, C.; Norgren, S. *Appl. Surf. Sci.* **2006**, *252* (15), 5499–5503.
(12) Davoodi, A.; Farzadi, A.; Pan, J.; Leygraf, C.; Zhu, Y. *J. Electrochem. Soc.* **2008**, *155* (8), C474–C485.
(13) Davoodi, A.; Pan, J.; Leygraf, C.; Norgren, S. *Electrochim. Acta* **2007**, *52* (27), 7697–7705.
(14) Sklyar, O.; Kueng, A.; Kranz, C.; Mizaikoff, B.; Lugstein, A.; Bertagnolli, E.; Wittstock, G. *Anal. Chem.* **2005**, *77* (3), 764–771.
(15) Burt, D. P.; Wilson, N. R.; Janus, U.; Macpherson, J. V.; Unwin, P. R. *Langmuir* **2008**, *24* (22), 12867–12876.
(16) Kottke, P. A.; Fedorov, A. G. *J. Electroanal. Chem.* **2005**, *583* (2), 221–231.
(17) Gullo, M. R.; Frederix, P.; Akiyama, T.; Engel, A.; deRooij, N. F.; Staufer, U. *Anal. Chem.* **2006**, *78* (15), 5436–5442.
(18) Frederix, P.; Bosshart, P. D.; Akiyama, T.; Chami, M.; Gullo, M. R.; Blackstock, J. J.; Dooleweerdt, K.; de Rooij, N. F.; Staufer, U.; Engel, A. *Nanotechnology* **2008**, *19* (38), 10.
(19) Dickinson, E. J. F.; Streeter, I.; Compton, R. G. *J. Phys. Chem. B* **2008**, *112* (13), 4059–4066.
(20) Wittstock, G.; Sklyar, O.; Treutler, T. H.; Vlachopoulos, N. *Surf. Sci.* **2005**, *597* (1−3), 181–95.
(21) Zoski, C. G.; Mirkin, M. V. *Anal. Chem.* **2002**, *74* (9), 1986–1992.
(22) Zoski, C. G.; Liu, B.; Bard, A. J. *Anal. Chem.* **2004**, *76* (13), 3646–3654.
(23) Daniele, S.; De Faveri, E.; Kleps, I.; Angelescu, A. *Electroanalysis* **2006**, *18* (18), 1749–1756.
(24) Avdic, A.; Lugstein, A.; Wu, M.; Gollas, B.; Pobelov, I.; Wandlowski, T.; Leonhardt, K.; Denuault, G.; Bertagnolli, E. *Nanotechnology* **2011**, in press.
(25) Bard, A. J.; Mirkin, M. V.; Unwin, P. R.; Wipf, D. O. *J. Phys. Chem.* **1992**, *96* (4), 1861–1868.
(26) Selzer, Y.; Mandler, D. *Anal. Chem.* **2000**, *72* (11), 2383–2390.
(27) Fulian, Q.; Fisher, A. C.; Denuault, G. *J. Phys. Chem. B* **1999**, *103* (21), 4387–4392.
(28) Sklyar, O.; Wittstock, G. *J. Phys. Chem. B* **2002**, *106* (30), 7499–7508.
(29) Sklyar, O.; Trauble, M.; Zhao, C. A.; Wittstock, G. *J. Phys. Chem. B* **2006**, *110* (32), 15869–15877.
(30) Abercrombie, S. C. B.; Denuault, G. *Electrochem. Commun.* **2003**, *5* (8), 647–656.
(31) Shin, H.; Hesketh, P. J.; Mizaikoff, B.; Kranz, C. *Anal. Chem.* **2007**, *79* (13), 4769–4777.